



Solid-state deposition of Mo-doped CoCrFeNi high-entropy alloy with excellent wear resistance via cold spray



Ningsong Fan^a, Tao Chen^b, Jiang Ju^c, Aran Rafferty^d, Rocco Lupoi^a, Ning Kong^{e, **}, Yingchun Xie^{f, ***}, Shuo Yin^{a,*}

^a Department of Mechanical, Manufacturing & Biomedical Engineering, Parsons Building, Trinity College Dublin, The University of Dublin, Dublin 2, Ireland

^b State Key Laboratory of Metastable Materials Science and Technology, Yanshan University, Qinhuangdao, 066004, China

^c Department of Materials Science and Engineering, College of Science and Engineering, City University of Hong Kong, Hong Kong, China

^d AMBER Centre, Trinity College Dublin, The University of Dublin, Dublin 2, Ireland

^e School of Mechanical Engineering, University of Science and Technology Beijing, Beijing, 100083, China

^f The Key Lab of Guangdong for Modern Surface Engineering Technology, National Engineering Laboratory for Modern Materials Surface Engineering Technology, Institute of New Materials, Guangdong Academy of Sciences, 510651, Guangzhou, China

ARTICLE INFO

Keywords:

Cold spray
High-entropy alloy
Microstructure
Wear resistance

ABSTRACT

To improve the wear resistance of CoCrFeNi high-entropy alloys (HEAs) for a wider range of industrial applications, the alloying strategy was applied to CoCrFeNi HEA by doping Mo element in various ratios, and CoCrFeNiMo_x ($x = 0, 0.2, 0.5$, and 1.0) HEA deposits were fabricated by cold spray. The microstructure evolution, mechanical properties, and tribological properties of cold-sprayed CoCrFeNiMo_x HEA deposits were systematically investigated. The results showed that Mo₀, Mo_{0.2}, and Mo_{0.5} deposits have a face-centered-cubic (FCC) single structure, while Mo_{1.0} deposit was composed of FCC matrix and hard brittle phases. The doping of Mo element into CoCrFeNi HEA deposits significantly increased the hardness due to the enhanced solid solution strengthening and precipitation strengthening. As a result, the anti-wear properties of Mo-doped CoCrFeNi HEA deposits were gradually improved with the increase in Mo ratios. To be specific, the Mo_{1.0} deposit exhibited the lowest specific wear rate of 5.1×10^{-5} mm³/N·m, which was reduced by 94.9% in comparison to the Mo₀ deposit. Overall, the current study proposes a new strategy to manipulate the mechanical properties of cold-sprayed HEA deposits by alloying.

1. Introduction

High-entropy alloys (HEAs) are a type of advanced multi-component alloys that are composed of five or more principal elements with an equiatomic or near equiatomic ratio [1]. The alloys obtained by mixing multiple elements in near/equal ratio form simple solid-solution structures rather than complex intermetallics. The unique multi-principal element compositions enable HEAs to exhibit a combination of high entropy, sluggish diffusion, severe lattice distortion, and cocktail effects, bringing HEAs excellent mechanical properties (e.g., high strength, high hardness), superior wear resistance, corrosion resistance, and high temperature resistance [1–6]. These excellent properties make HEAs a potential substitute for conventional alloys used in aerospace, energy,

electronics, and medical fields [3].

One of the promising applications of HEAs is serving as protective coatings to protect the surface of parts from wear and corrosion, particularly under harsh working conditions. To date, various techniques, such as laser cladding [7,8], magnetron sputtering [9], electro spark deposition [10], and thermal spray [11,12], have been utilized to prepare HEA coatings. Cold spray, as a promising solid-state material deposition technique, offers an alternative route to fabricate HEA coatings [13–15]. In cold spray process, micro-sized feedstock powder is accelerated to supersonic velocities in a de-Laval nozzle by a compressed and heated stream of nitrogen or helium gas before impacting toward a substrate. The particles experience extreme and rapid plastic deformation upon impact and form a strong bond with a substrate or previously

* Corresponding author.

** Corresponding author.

*** Corresponding author.

E-mail addresses: kongning@ustb.edu.cn (N. Kong), xieyingchun@gdinm.com (Y. Xie), yins@tcd.ie (S. Yin).

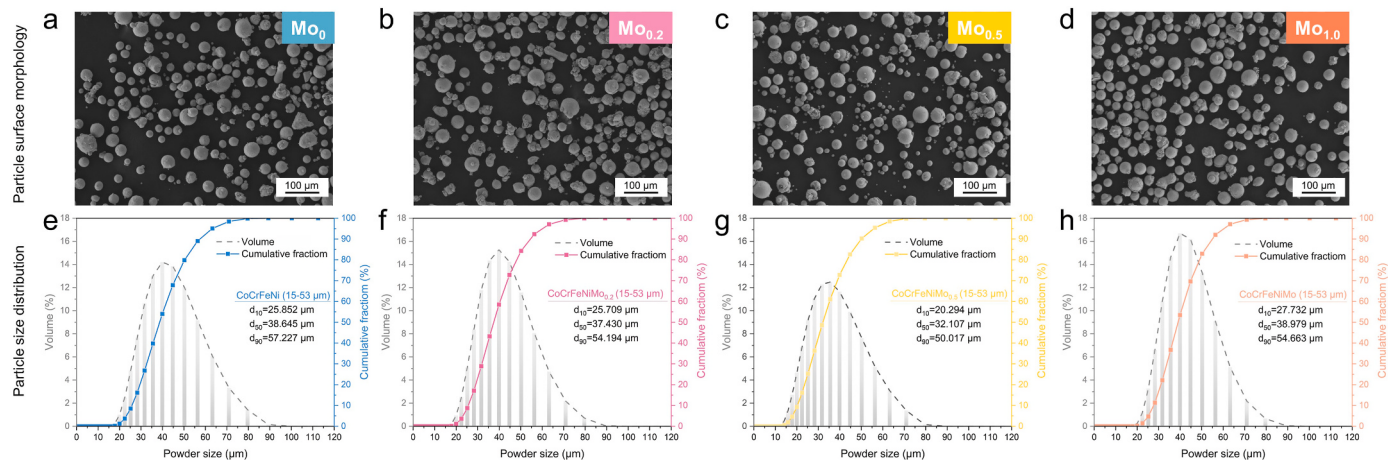


Fig. 1. Surface morphology and particle size distribution of the gas-atomized CoCrFeNiMo_x HEA feedstock for deposit fabrication. (a, e) Mo₀, (b, f) Mo_{0.2}, (c, g) Mo_{0.5}, and (d, h) Mo_{1.0}.

Table 1

Nominal and measured element composition of the CoCrFeNiMo_x HEA feedstock.

Feedstock powder	Composition	Element/at%				
		Co	Cr	Fe	Ni	Mo
CoCrFeNi	Nominal	25.00	25.00	25.00	25.00	/
	Actual	24.25	25.08	25.60	25.06	/
CoCrFeNiMo _{0.2}	Nominal	23.81	23.81	23.81	23.81	4.76
	Actual	23.73	23.92	23.88	23.68	4.79
CoCrFeNiMo _{0.5}	Nominal	22.22	22.22	22.22	22.22	11.11
	Actual	21.96	22.19	22.58	22.08	11.19
CoCrFeNiMo _{1.0}	Nominal	20.00	20.00	20.00	20.00	20.00
	Actual	19.43	19.32	19.25	19.40	22.60

deposited layers through mechanical interlocking and localized metallurgical bonding at highly deformed interfacial regions. The formation of cold-sprayed deposits relies on high kinetic energy rather than thermal energy, which helps to minimize thermal influences (e.g., oxidation, phase transformation, residual thermal stress and grain growth) [16]. In

addition, the working hardening effect induced by the severe plastic deformation of particles leads to a significant increase in hardness, implying the superior wear-resistant properties of the deposits [17,18]. Moreover, cold spray deposition process does not produce any harmful fumes or gases, making it more environmentally friendly compared with thermal spray and other melting-solidification manufacturing techniques.

CoCrFeNi is a representative HEA system with a single face-centered cubic (FCC) solid solution structure, which has been well explored in the last decade due to its good ductility [19–21]. However, it has relatively low strength and hardness, which presents a major concern for its use of wear-resistant materials particularly in extreme environments (e.g., high loads and high temperatures). One commonly used strategy to manipulate the mechanical properties of HEAs is to carefully adjust the alloying elements and composition to confer secondary properties. Molybdenum is primarily used as an alloying agent in steel to increase strength, hardness, hardenability, and toughness, as well as enhance resistance to corrosion, heat, and wear [22]. Recent studies have shown that the addition of Mo element with appropriate proportion into the

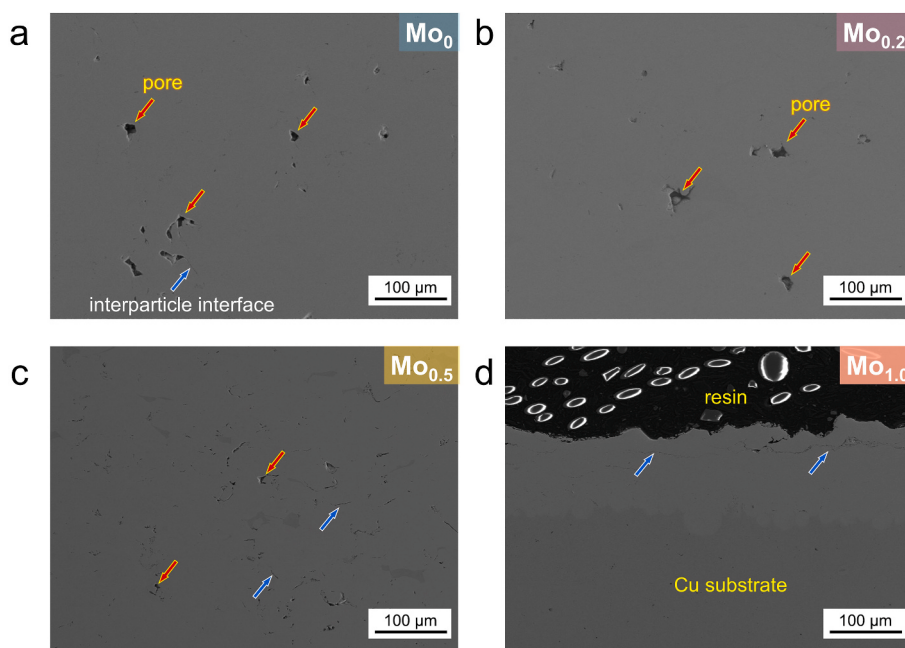


Fig. 2. Cross-sectional microstructure of the cold-sprayed CoCrFeNiMo_x HEA deposits. (a) Mo₀, (b) Mo_{0.2}, (c) Mo_{0.5}, (d) Mo_{1.0}.

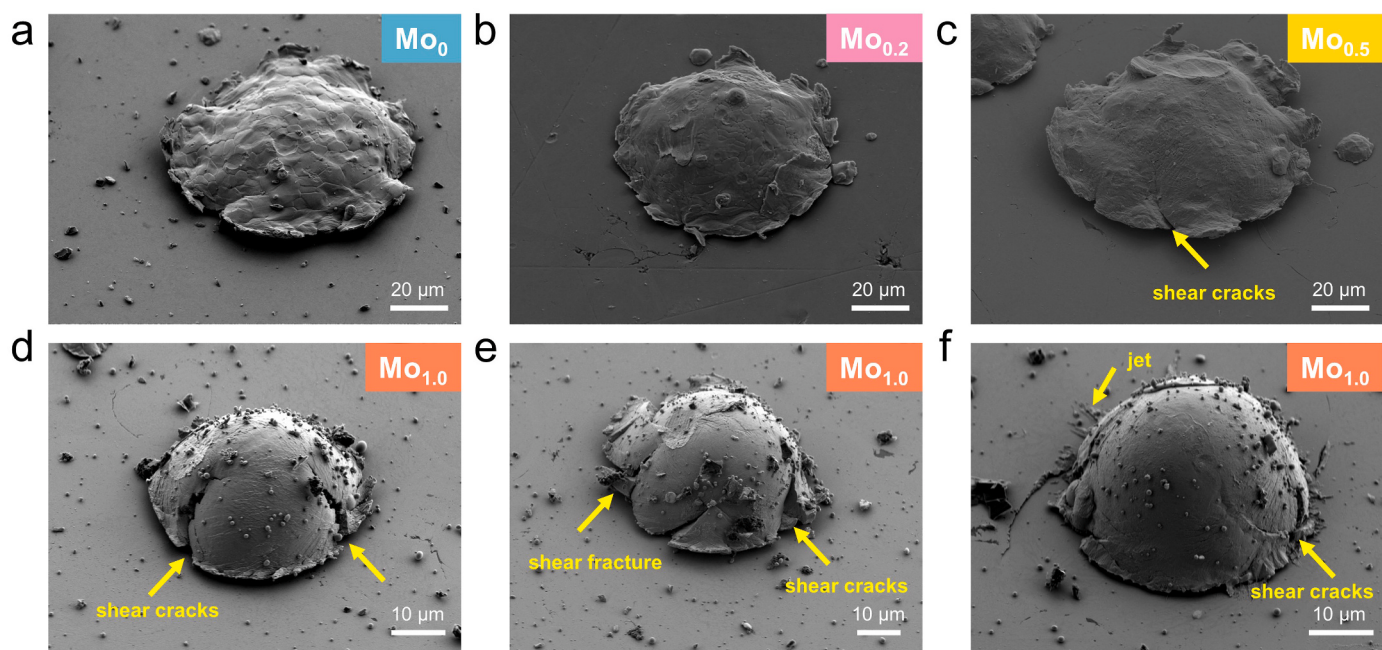


Fig. 3. Representative surface morphologies of individual deposited CoCrFeNiMo_x HEA particles. (a) Mo₀, (b) Mo_{0.2}, (c) Mo_{0.5}, (d–f) Mo_{1.0}. Note the substrate used in single particle deposition is the polished cold-sprayed CoCrFeNiMo_x HEA deposits.

CoCrFeNi HEA system has demonstrated the improvement of mechanical properties [23–25]. When the content of Mo added in the CoCrFeNi HEA is relatively low, the high mixing entropy effect brought by the multi-principal component effectively inhibits the phase separation, resulting in a single solid solution structure. Mo is dissolved in the lattice structure of the FCC matrix in the form of substitutional atoms, which increases the lattice distortion of the alloy due to its large atomic radius and thus strengthens the CoCrFeNi HEA. A further increase of Mo will promote the precipitation of hard and brittle topologically close-packed (TCP) phases: (Cr, Mo)-rich sigma (σ) phase and (Mo, Cr)-rich mu (μ) phase in the matrix [23,24]. The precipitation of such phases results in significantly enhanced hardness and strength through solution strengthening and precipitation strengthening mechanisms, which makes CoCrFeNiMo HEA alloy excellent wear-resistant material candidates [23,25]. However, the precipitation of σ and μ phases also embrittles the materials, which leads to the loss of ductility. This means that insufficient plastic deformation of particles and extremely low deposition efficiency will likely occur during the cold spray deposition process if a high content of Mo element doped CoCrFeNi HEA is directly used as feedstock powder. Therefore, in the present work, gas-atomized CoCrFeNiMo_x HEA powders with different Mo ratios were used as feedstock, and the effect of Mo element on the microstructure and wear-resistance properties of the cold-sprayed CoCrFeNiMo_x HEA deposits was systematically explored. The results of this study show that the regulation of the Mo elemental ratios can significantly enhance the wear-resistant properties of the cold-sprayed CoCrFeNi HEA deposits. However, the increase of the Mo content will influence the deposition behaviors of particles, and the content of Mo in CoCrFeNiMo_x HEA needs to be balanced against the depositability of the material.

2. Material and methodology

2.1. Feedstock powder

Gas-atomized CoCrFeNiMo_x ($x = 0, 0.2, 0.5$, and 1.0) HEA powders with a nominal particle size distribution of 15–53 μm were used as feedstock. Fig. 1 shows the surface morphology and particle size distribution of the HEA powders. The particle surface morphology was

characterized by scanning electron microscope (SEM, Carl Zeiss Ultra Plus, Germany). Most powders featured high sphericity. The size distribution of the powder was measured by a laser diffraction particle analyzer (Mastersizer 2000, Malvern Instruments, UK). The actual element composition of the CoCrFeNiMo_x HEA powders was examined by inductively coupled plasma optical emission spectroscopy (ICP-OES, Prodigy XP, Leeman, US), as listed in Table 1.

2.2. Cold spray process

A commercial high-pressure cold spray system (PCS-1000, Plasma Giken, Japan) was used for CoCrFeNiMo_x HEA deposit fabrication. Compressed nitrogen was used as propelling gas, and the inlet pressure and temperature were kept at 5.0 MPa and 900 °C, respectively. A square Cu plate with a size of 100 mm × 100 mm × 3.0 mm was used as the substrate, and the substrate surface was ground with sandpaper prior to cold spraying to remove oxide film and improve adhesion strength, followed by cleaning with anhydrous ethanol. The standoff distance from the exit of the nozzle to the Cu substrate surface remained 40 mm during the deposition. The nozzle moving trajectory followed a reciprocating zigzag strategy, and the space between two neighboring tracks was 1.0 mm. The deposits were subsequently processed into cubes (15 mm × 15 mm × 5 mm) by a wire-cutting electrical discharge machine (EDM, V400G, Exectek V400G, China) for the following wear-resistance property evaluation. To investigate the deposition behavior of CoCrFeNiMo_x HEA particles, individual splat was deposited onto mirror-polished cold-sprayed CoCrFeNiMo_x HEA deposits under a nozzle traversal speed of 320 mm/s. The surface morphology of the single splat was characterized by SEM.

2.3. Microstructure Characterization

The cross-sectional samples were mechanically ground and polished following metallurgical procedures for microstructure analysis. The density of the deposits was evaluated from optical microscopy (Leica DM LM, Germany) images using an image analysis method based on ASTM E2109-01 standard. The result was averaged from ten different deposit regions to ensure data reliability. To identify phase composition, both

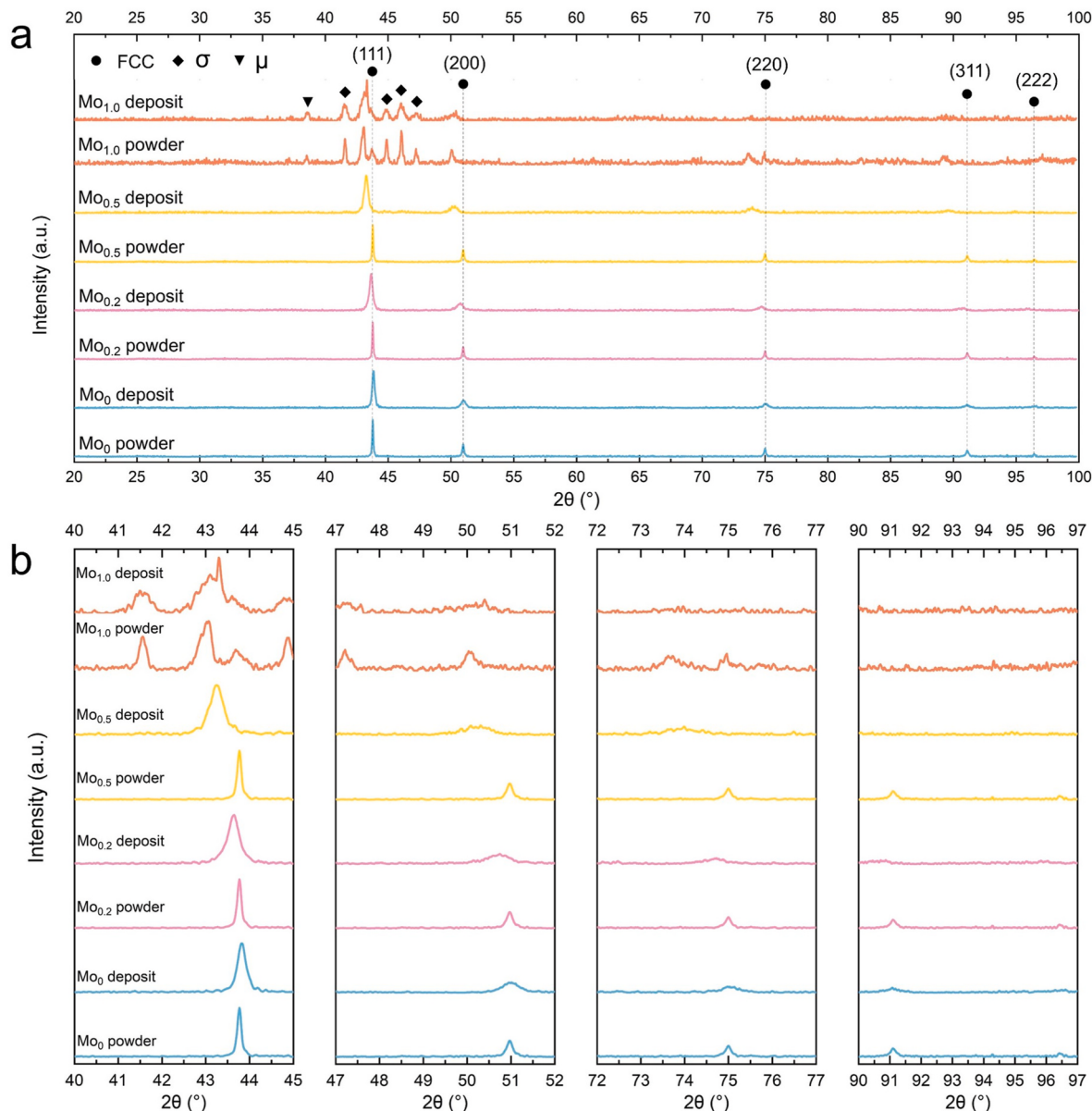


Fig. 4. X-ray diffraction (XRD) analysis of the CoCrFeNiMo_x HEA feedstock powder and the cold-sprayed deposits in the range of 20°–100°. (a) XRD patterns, (b) Magnified patterns of main peaks.

the feedstock powders and deposits were analyzed by X-ray diffraction (XRD, X'pert Powder, PANalytical, Netherlands) equipped with Cu-K α radiation from a range of 2 θ values between 20° and 100° (40 kV, 40 mA) with a scanning step size of 0.013.

2.4. Mechanical properties measurement

Depth sensing indentation test was carried out on the cross-section of the cold-sprayed CoCrFeNiMo_x HEA deposits using a nanoindenter (MTS Nanoindenter XP, USA) equipped with a Berkovich triangular diamond tip at ambient temperature. The equipment has a high displacement resolution (<0.01 nm) and load resolution (50 nN). A matrix of 10 × 6 indentations was conducted along the deposition direction with a depth limit of 1000 nm. The region without pores or cracks was selected for testing to avoid the effect of defects on the true indentation value of the deposits. The interval between each indentation in both horizontal and vertical directions was spaced at 20 μ m to avoid potential interactions between strain fields of adjacent indentations. The load on the sample and its corresponding displacement into the surface were recorded as a

function of time during the nanoindentation test. The hardness and elastic modulus of the deposit were obtained automatically from the system based on the Oliver-Pharr methodology [26]. The typical micrographs of indentations were then characterized by SEM.

The wear-resistance properties of the cold-sprayed CoCrFeNiMo_x HEA deposits were evaluated by a ball-on-disk reciprocating tribometer (MFT-5000, RTEC, USA) at ambient temperature. The GCr15 steel ball (also known as AISI 52100 alloy steel) with a diameter of 4.0 mm was used as the counterpart. A constant normal load of 20 N was applied on the mirror-polished deposit surface during the test with an oscillating frequency of 4.0 Hz and a stroke length of 5.0 mm. The test lasted 30 min, and at least three tests were run for each sample to ensure the data reliability. The coefficient of friction (COF) versus time was automatically recorded by the tribometer. The three-dimensional (3D) topography of the wear track was constructed using a 4 K ultra-high accuracy digital microscope (VHX-7000 N, Keyence, Japan), and the wear volume can be calculated automatically by the software. The specific wear rate was quantified according to Archard's wear law [27], which can be defined as

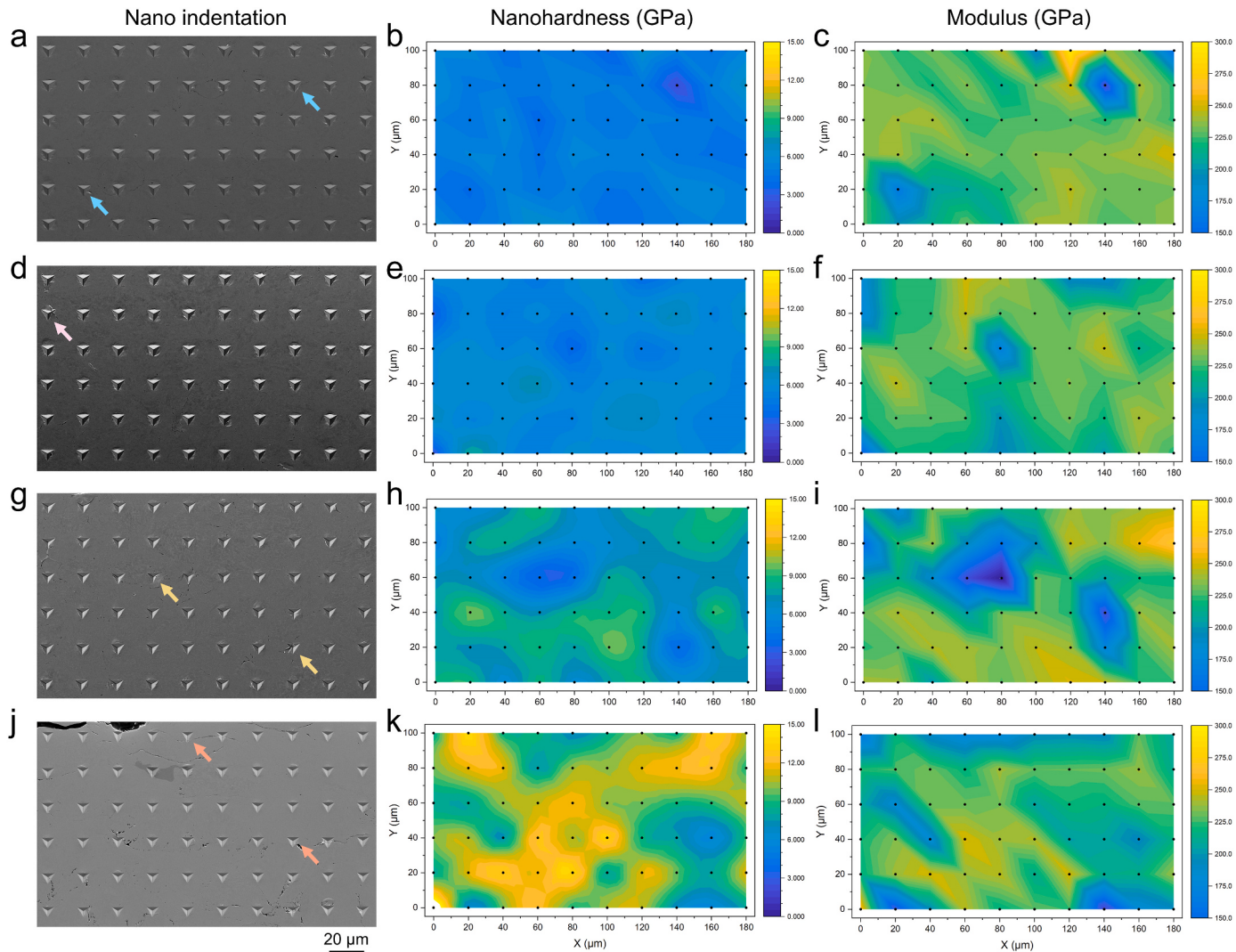


Fig. 5. Nanoindentation (left column), nano-hardness (middle column) and modulus (right column) mapping obtained from 10×6 nanoindentation grids on the polished cross-sectional CoCrFeNiMo_x HEA samples fabricated by cold spray. (a, b, c) Mo₀, (d, e, f) Mo_{0.2}, (g, h, i) Mo_{0.5}, (j, k, l) Mo_{1.0}.

$$w = \frac{v}{FS}$$

where W is the wear rate ($\text{mm}^3/\text{N}\cdot\text{m}$), V is the wear volume (mm^3), F is the applied normal load (N), and S is the total sliding distance (m). The surface morphology, cross-sectional morphology, and chemical composition of the worn tracks were characterized by SEM and EDS to analyze the wear mechanisms.

3. Results and discussion

3.1. Microstructure, deposition behavior and phase structure

Fig. 2 shows the cross-sectional microstructure of the cold-sprayed CoCrFeNiMo_x HEA deposits. Micropores and incomplete particle bonding can be observed in the deposits, which are the typical manufacturing defects in cold-sprayed deposits. Such defects are generally associated with the insufficient plastic deformation of HEA particles during the deposition. The relative density of the CoCrFeNiMo_x HEA deposits was estimated to be $98.62 \pm 0.49\%$ (Mo₀), $98.05 \pm 0.23\%$ (Mo_{0.2}), $97.99 \pm 0.25\%$ (Mo_{0.5}) and $97.98 \pm 0.72\%$ (Mo_{1.0}) respectively. The relative density shows a downward trend, which can be attributed to the increased plastic deformation resistance with the increased Mo ratio in CoCrFeNiMo_x HEA deposits. In addition, it is

notable that the thickness of the Mo_{1.0} deposit is only around 0.1 mm in comparison to the thick Mo₀, Mo_{0.2}, and Mo_{0.5} deposits. This suggests that the deposition of Mo_{1.0} HEA powder is rather difficult, even though high processing parameters were used.

Fig. 3 shows the representative surface morphologies of individual CoCrFeNiMo_x HEA particles deposited onto polished cold-sprayed CoCrFeNiMo_x HEA deposits. The spherical Mo₀ particle (see Fig. 3a) was flattened after high-velocity impact, suggesting the good ductility of the material. This also happened to Mo_{0.2} and Mo_{0.5} particles, as evidenced by the severely plastic deformed particles in Fig. 3b and c. The sufficient plastic deformation of particles contributes to the fabrication of deposits with fewer defects and better interparticle bonding. While for the Mo_{1.0} particles, the deposited particles were nearly hemispherical in shape, and shear cracks and fractures were visible, implying the brittle feature of the material. Such difference can be attributed to the increased deformation resistance with the increased Mo ratio in the CoCrFeNiMo_x HEA particles. It is reported that the as-casted Mo₀ HEA presented a compressive yield strength of 207 MPa and a 60% engineering strain without failure. While the compressive yield strength significantly increased to 825 MPa for Mo_{1.0} HEA due to the solid solution strengthening and precipitation strengthening, but the fracture strain was as low as 11.4% [25]. This is consistent with the brittle characteristics of the deposited Mo_{1.0} particles, as shown in Fig. 3d-f.

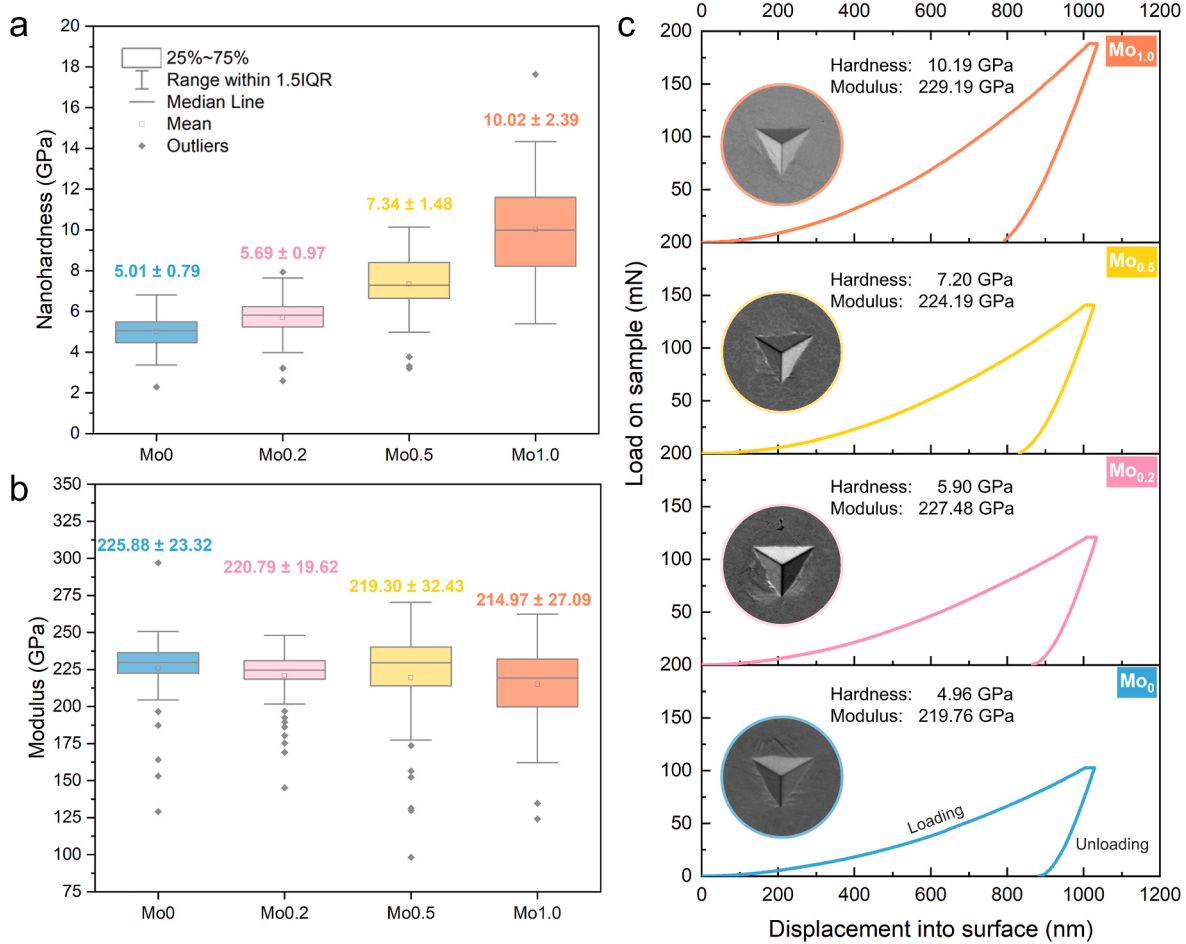


Fig. 6. (a) Nanohardness, (b) Modulus, and (c) Representative load-displacement curves of the cold-sprayed CoCrFeNiMo_x HEA deposits from the nano-indentation tests.

Table 2

Summary of Hardness (H), Modulus (E), H/E and H³/E² values of the cold-sprayed CoCrFeNiMo_x HEA deposits from the nanoindentation test.

Deposit	H (GPa)	E (GPa)	H/E	H ³ /E ² (GPa)
Mo ₀	5.01 ± 0.79	225.88 ± 23.32	0.022 ± 0.004	0.003 ± 0.001
Mo _{0.2}	5.69 ± 0.97	220.79 ± 19.62	0.026 ± 0.004	0.004 ± 0.002
Mo _{0.5}	7.34 ± 1.48	219.30 ± 32.43	0.033 ± 0.004	0.009 ± 0.003
Mo _{1.0}	10.02 ± 2.39	214.97 ± 27.09	0.046 ± 0.007	0.023 ± 0.013

The impact of subsequent particles onto the previous deposited layers or particles could lead to further particle fracture. The high deformation resistance and the brittle characteristics led to the low deposition efficiency of the Mo_{1.0} HEA deposit under the current processing parameters, and the thickness of the deposit was limited to about 0.1 mm, as shown in Fig. 2d.

Fig. 4 displays the XRD spectrum of the CoCrFeNiMo_x HEA feedstock powder and the cold-sprayed deposits. The Mo₀ deposit is identified as a single FCC solid solution structure as the original Mo₀ feedstock powder. However, the deposit shows a broadening in the peaks compared with the powder (see the enlarged XRD pattern in Fig. 4b), which can be attributed to the increased lattice defects and the refined grains induced by severe plastic deformation during the deposition process [28]. The Mo_{0.2} powder and corresponding deposit are also indexed as FCC phase, but the diffraction peaks shifted toward lower diffraction angles compared with Mo₀ powder and deposit, indicating the increase in lattice parameters. Due to the large atomic size difference between Mo and the other four elements (i.e., Co-0.125 nm, Cr-0.128 nm, Fe-0.126 nm,

Ni-0.124 nm, and Mo-0.139 nm), the doping of Mo into CoCrFeNi HEA leads to lattice distortion [29]. This can also be demonstrated by the lattice constant of Mo₀ and Mo_{0.2} deposits, which are determined to be 3.5577 Å and 3.5912 Å, respectively. The Mo_{0.5} and corresponding deposit were also identified as a single FCC solid solution structure, which was inconsistent with previous studies. It is reported that the as-casted CoCrFeNiMo_{0.5} HEA was composed of FCC and hard brittle σ phase, and the σ phase appeared near the diffraction peak of the (111) plane [30,31]. Such difference is believed to be associated with the different manufacturing processes. Compared with the casting method, the microstructure of the cold-sprayed deposits is more refined, and the size and content of the σ phase may exceed the detection limit of XRD. The increase in the Mo ratio resulted in more severe lattice distortion, as evidenced by the lattice parameter of Mo_{0.5} (3.6227 Å). The lattice distortion induced by the atomic size mismatch can lead to enhanced solid solution strengthening, which will hinder the movement of dislocation and lead to improved wear resistance. For the Mo_{1.0} feedstock powder and deposit, the hard and brittle sigma (σ) phase and mu (μ) phase were identified, as shown in Fig. 4a. The valence electron concentration (VEC) is regarded as a useful parameter to predict the stability of solid solution phases in HEAs, which can be expressed as:

$$VEC = \sum_i^n C_i VEC_i$$

where C_i is the atomic percentage of each element in HEA, and VEC_i is the VEC of each element. The VEC for CoCrFeNiMo_x HEA is calculated to be 8.25 (Mo₀), 8.14 (Mo_{0.2}), 8.00 (Mo_{0.5}), and 7.80 (Mo_{1.0}) respectively.

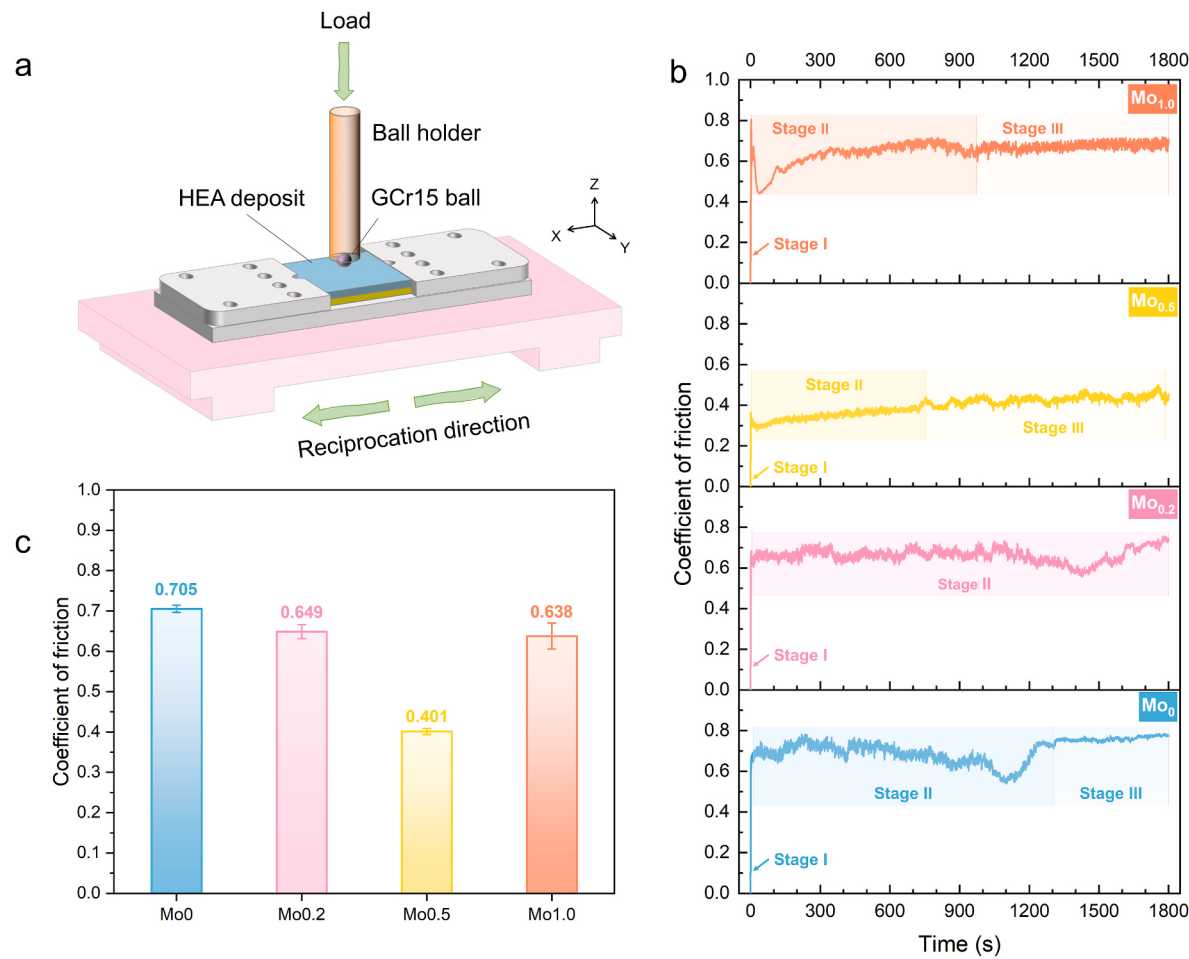


Fig. 7. Dry-sliding wear behavior of the cold-sprayed CoCrFeNiMo_x HEA deposits. (a) Schematic diagram of the reciprocating sliding friction and wear test, (b) Representative plots of COF as a function of sliding time, (c) Coefficient of friction (COF) averaged from three tests. The main parameters for the dry sliding wear test include normal load (20 N), oscillating frequency (4.0 Hz), stroke length (5.0 mm), and time of duration (30 min).

It was reported that FCC is stable when VEC ≥ 8 , while BCC is stable when VEC ≤ 6.87 [32,33]. Moreover, the formation of σ phase in Cr-containing HEAs is expected when the VEC is between 6.88 and 7.84 [34]. The formed σ and μ phases are believed to further improve the mechanical performance of the Mo_{1.0} deposit.

3.2. Nanohardness

Fig. 5 displays the SEM images of the indentation matrix and corresponding contour maps of nanohardness and modulus versus position. It is observed that all the deposits exhibited microscale heterogeneity, as indicated by the color variability in the hardness mapping. On the one hand, due to the existence of particle-particle boundaries and the micropores, the indentation near these defects (as indicated by the arrows) exhibited lower hardness and modulus. On the other hand, the high-velocity impact of the originally spherical particle led to significant strain, strain rate, and temperature gradients during severe plastic deformation and the resultant heterostructure. Specifically, ultra-fine grains usually form near interfacial regions due to grain fragmentation and dynamic recrystallization, while elongated and flattened grains remain in the particle interior. Such cross-scale grain structure led to the heterogeneous mechanical properties at different positions.

Fig. 6 shows the average nanohardness, modulus, and representative load-displacement curves of the cold-sprayed CoCrFeNiMo_x HEA deposits during loading-unloading nanoindentation tests. The nanohardness increased from 5.01 ± 0.79 GPa to 10.2 ± 2.39 GPa with the increase in Mo ratio from 0 to 1.0 in CoCrFeNiMo_x HEA deposits, as

shown in Fig. 6a. The nanohardness of the Mo_{0.2} and Mo_{0.5} deposits are 5.69 ± 0.97 GPa and 7.34 ± 1.47 GPa, respectively. Such a trend is in line with the previous study that the increase of Mo addition leads to the increased hardness in the CoCrFeNiMo_x HEAs [29,30]. On the one hand, cold-sprayed deposits generally exhibited higher hardness than their counterparts due to the significant work hardening induced by severe plastic deformation. On the other hand, the doping of Mo into CoCrFeNi HEA deposits led to the lattice distortion of the FCC structure due to its larger atom size, which can be confirmed by the increased lattice constant calculated from the XRD data (see Fig. 6). Moreover, the hard σ and μ intermetallic precipitated in the FCC matrix further contributed to the high hardness of the Mo_{1.0} deposit. The modulus of Mo₀ reached 225.88 ± 23.32 GPa, and it slightly decreased to 220.79 ± 19.62 GPa (Mo_{0.2}), 219.30 ± 32.43 GPa (Mo_{0.5}) and 214.97 ± 27.09 GPa (Mo_{1.0}) respectively with the increase of Mo ratio in CoCrFeNiMo_x HEA deposits, as shown in Fig. 6b.

It is reported that the ratio between hardness (H) and modulus (E) can be taken as a parameter to predict the wear resistance of a material (e.g., elastic strain to failure, the critical yield stress for plastic deformation, and the fracture toughness) [35]. The ratio of hardness to elastic modulus (H/E) is related to the elastic strain to failure capability. The H/E of the cold-sprayed CoCrFeNiMo_x HEA deposits shows a near-linear increased trend with the increased ratio of Mo element. The H³/E² ratio, also known as the plasticity index, can be considered as a parameter to describe the resistance to plastic deformation [35]. The H³/E² value of the Mo_{1.0} deposit reached 0.023 GPa, which is 86.96% higher than that of the Mo₀ deposit and 60.87% higher than that of the Mo_{0.5} deposit,

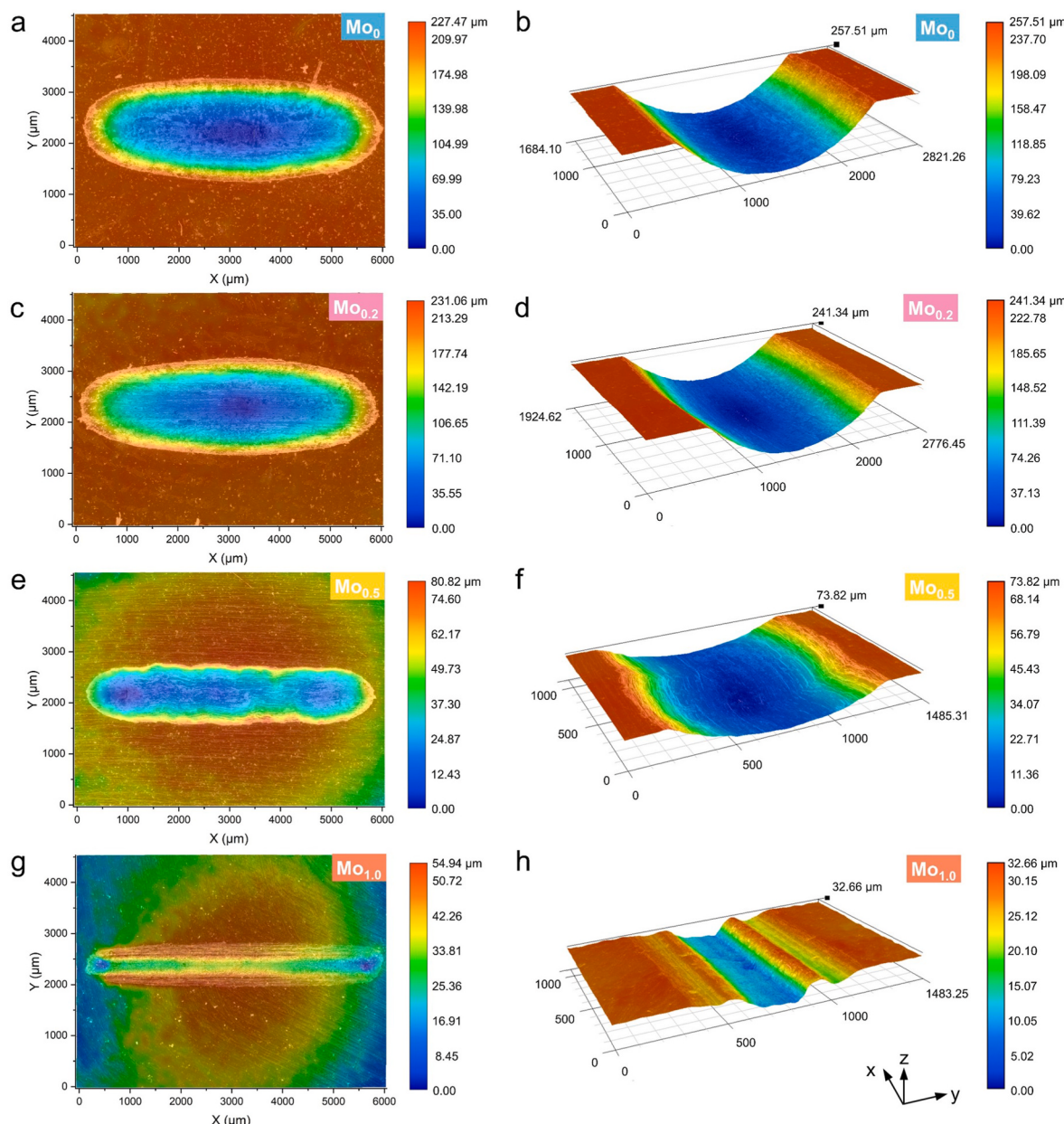


Fig. 8. 2D surface morphology (left side) and 3D topography (right side) of the wear tracks on the cold-sprayed CoCrFeNiMo_x HEA deposits. (a, b) Mo₀, (c, d) Mo_{0.2}, (e, f) Mo_{0.5}, (g, h) Mo_{1.0}.

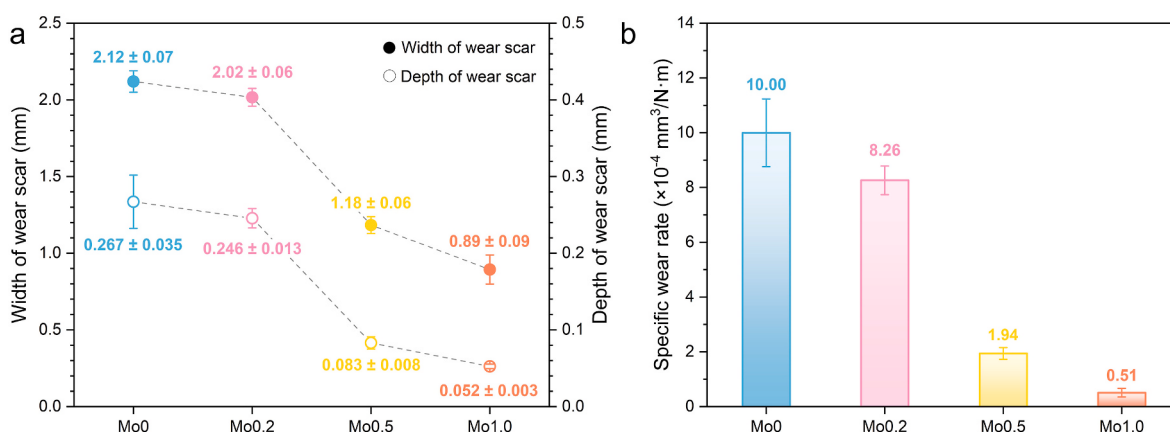


Fig. 9. (a) The maximum width and depth of the wear tracks and (b) The specific wear rate of the cold-sprayed CoCrFeNiMo_x HEA deposits.

Table 3

Summarization of the specific wear rate of CoCrFeNiMo_x HEA samples fabricated by different manufacturing routes.

Raw material	Manufacturing routes	Specific wear rate (mm ³ /N-m)	Ref
Mo ₀	FeCoNiCr and Mo powders	Ball milling + Laser cladding	0.36 [38]
Mo _{0.15}			0.32
Mo _{0.2}			0.26
Mo _{0.25}			0.22
Mo ₀	Spherical HEA powders	Spark plasma sintering + Cold rolling	0.42 × 10 ⁻³ [29]
Mo _{0.1}			0.36 × 10 ⁻³
Mo _{0.3}			0.33 × 10 ⁻³
Mo _{1.0}	Gas-atomized powder	Laser cladding	~3 × 10 ⁻⁵ [39]
Mo ₀	Pure metal powders	Mechanically mixing + Laser cladding	3.54 × 10 ⁻⁴ [40]
Mo _{0.5}			2.43 × 10 ⁻⁴
Mo ₁			1.91 × 10 ⁻⁴
Mo _{1.5}			1.1 × 10 ⁻⁴
Mo _{0.2}	Pure metal powders	Casting + High-current pulsed electron beam	0.92 × 10 ⁻⁴ ~ [41]
Mo ₀	Pure metal powders	Casting	6.07 × 10 ⁻⁴ [25]
Mo _{0.3}			~8.50 × 10 ⁻⁴
Mo _{0.5}			~5.85 × 10 ⁻⁴
Mo ₁			~1.68 × 10 ⁻⁴
Mo _{1.5}			~0.83 × 10 ⁻⁴
Mo _{0.5}	Gas-atomized powder	Plasma spraying	1.27 × 10 ⁻⁴ [42]
Mo _{0.2}	Pure metal powders	Ball milling + Laser cladding	1.33 × 10 ⁻³ [43]
Mo ₀	Pure metal powders	Ball milling + Laser cladding	0.76 [37]
Mo _{0.3}			0.64
Mo _{0.6}			0.44
Mo _{0.9}			0.40
Mo _{1.2}			0.29

respectively, as summarized in **Table 2**. This suggests that the Mo_{1.0} deposit exhibits high plastic deformation resistance and is expected to show superior wear resistance than the other deposits.

3.3. Wear resistance properties

Fig. 7 shows the dry-sliding wear behavior of the cold-sprayed CoCrFeNiMo_x HEA deposits. The working principle of the tribometer used for dry-sliding wear behavior investigation was provided in **Fig. 7a**. The ball remains stationary while the platform together with the specimen reciprocates along the x-direction during the test. **Fig. 7b** plots the COF evolution history of the CoCrFeNiMo_x HEA deposits. All the deposits exhibit a running-in process (stage I) at the initial stage of the wear test [36], which is the result of contacting between micro-protrusions or asperities on the surface of the friction pair (i.e., GCr15 ball/CoCrFeNiMo_x HEA deposits). This two-body abrasion leads to a rapid increase in COF. In stage II, the COF fluctuated with time particularly for the Mo₀ and Mo_{0.2} specimens. This could be associated with the material removal from the friction pair, suggesting the poor wear resistance of the deposits. As the friction proceeded, wear debris was peeled off from the deposit surface and piled up between the two contacting surfaces, and the contact modes changed from two-body abrasion to three-body abrasion. For the Mo_{0.5} deposit, the fluctuation of COF was significantly weakened at stage II, exhibiting a slow upward trend in the range of 0.3 and 0.4. This could be attributed to the enhanced hardness of the deposit. The COF of the Mo_{1.0} deposit decreased after the running-in stage and steadily increased (stage II), with a higher COF level than that of the Mo_{0.5} deposit. In the late testing period (stage III), there is no obvious fluctuation of COF, particularly for Mo₀ and Mo_{1.0} deposits, which suggests the dynamic equilibrium of the

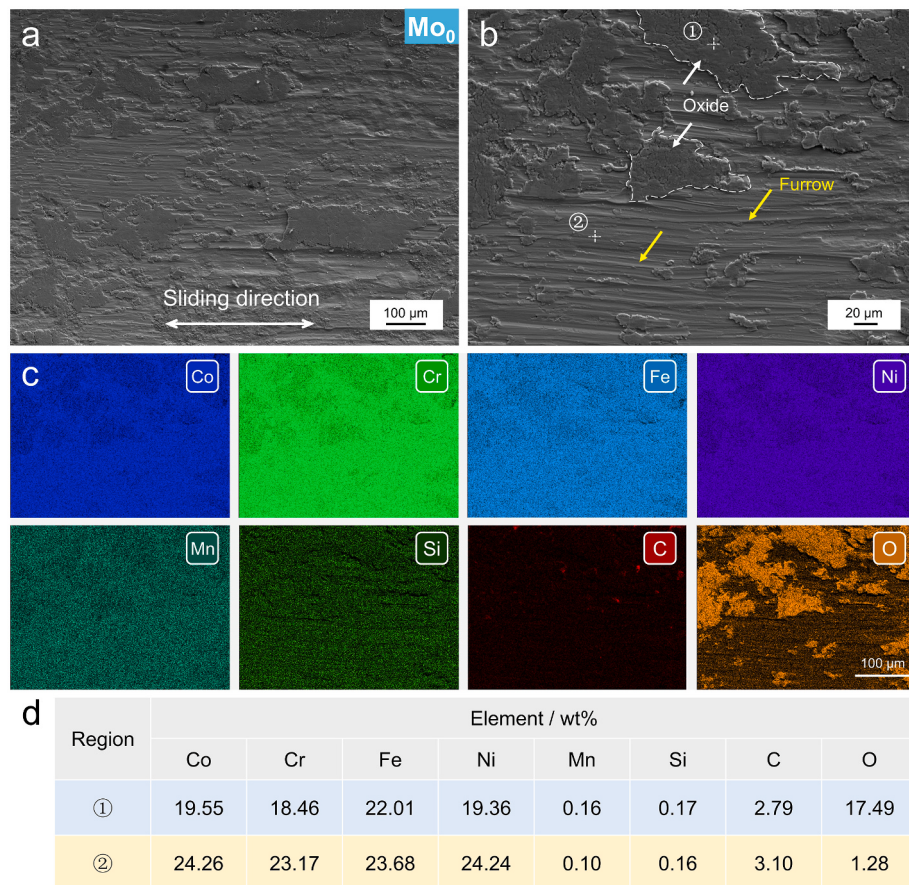


Fig. 10. Representative worn surface morphology and EDS results of the cold-sprayed CoCrFeNi HEA deposit. (a) and (b) SEM images, (c) and (d) EDS mapping and points analysis.

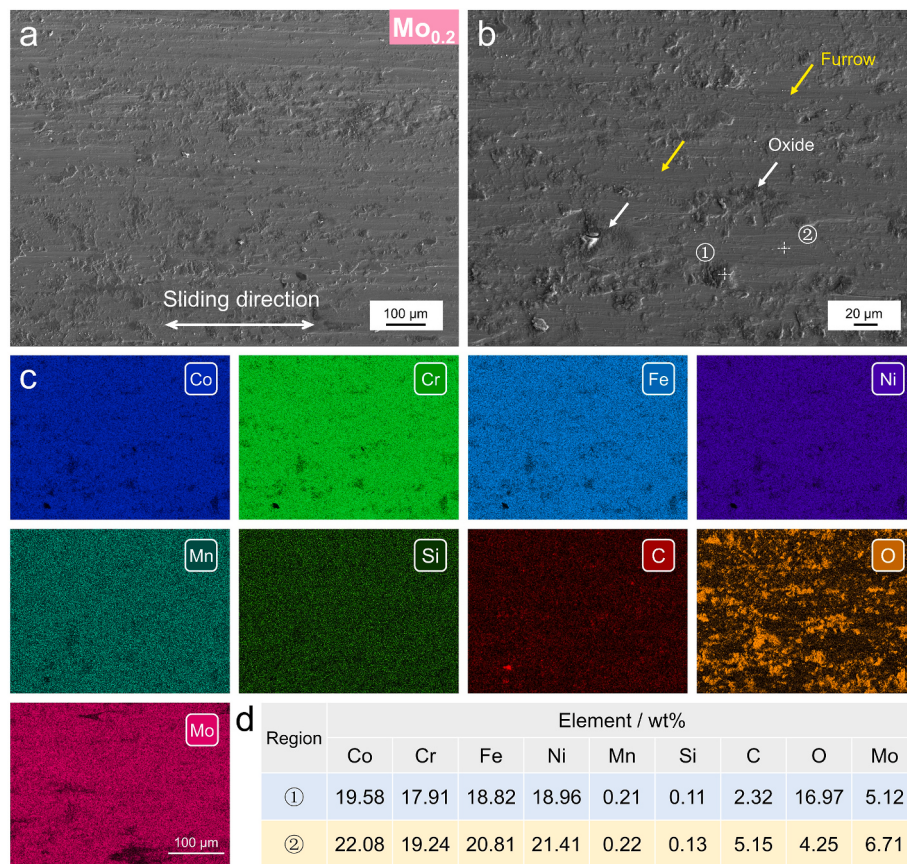


Fig. 11. Representative worn surface morphology and EDS results of the cold-sprayed CoCrFeNiMo_{0.2} HEA deposit. (a) and (b) SEM images, (c) and (d) EDS mapping and points analysis.

wear. However, the steady-wear stage was not found for the Mo_{0.2} deposit. The sudden drop and rise of COF before the test end could be associated with the peeling off from the Mo_{0.2} deposit, and it was expected that the COF would tend towards stability at stage III if the friction continued.

The average COF of the cold-sprayed CoCrFeNiMo_x HEA deposits based on the results of three tests was summarized in Fig. 7c. The Mo₀ deposit exhibits the highest COF among all the deposits, and the average COF is 0.705 ± 0.009 . With the increase of Mo ratio in the CoCrFeNiMo_x HEA deposits, the COF decreased to 0.649 ± 0.017 (Mo_{0.2}) and 0.401 ± 0.008 (Mo_{0.5}), respectively. This suggests that less friction force is required for the sliding on the Mo-doped CoCrFeNi HEA deposit against the GCr15 ball. However, a further increase in Mo content led to the increased COF to 0.638 ± 0.032 (Mo_{1.0}). The decrease followed by the rebound of COF with the increasing Mo ratio in CoCrFeNiMo_x HEA was also found in previous studies [25,37].

Fig. 8 exhibits the 2D surface morphology and the 3D topography of the representative wear tracks of the cold-sprayed CoCrFeNiMo_x HEA deposits. The different colors indicate the depth change of the wear surface. The wear tracks of the Mo₀ and Mo_{0.2} deposits are nearly elliptical in shape, and the closer to the center of the elliptical, the deeper the wear track is. The maximum width and depth of the wear tracks were measured based on the optical images, as plotted in Fig. 9a. Compared with the Mo₀ deposit, the maximum width was decreased from 2.12 mm to 2.02 mm, and the maximum depth was also decreased from 0.267 mm to 0.246 mm, suggesting the reduced wear volume and the improved resistance to material removal for the Mo_{0.2} deposit. The wear track of the Mo_{0.5} deposit exhibited a pill shape, and the width and depth of the wear track further decreased to 1.18 mm and 0.083 mm, respectively. The Mo_{1.0} deposit exhibited the narrowest and shallowest wear track among all the deposits, and the average maximum width and

depth were measured to be 0.89 mm and 0.052 mm. This implies that the doping of Mo element into CoCrFeNi HEA can significantly reduce the wear volume, which is associated with the increased hardness of the CoCrFeNiMo_x HEA deposits with the increased ratio of Mo element (see Fig. 8). According to Archard's law, the volume of the worn material is inversely proportional to the material hardness [27]. Moreover, the parameter H³/E² (as listed in Table 2) also shows an increasing trend with the increased Mo ratio, indicating the increased plastic deformation resistance and the enhanced wear resistance of the cold-sprayed CoCrFeNiMo_x HEA deposits.

For a more accurate description of the wear characteristic of the cold-sprayed CoCrFeNiMo_x HEA deposits, the specific wear rate (mm³/N·m) was calculated, as shown in Fig. 9b. The Mo₀ deposit exhibits the worst wear resistance with a specific wear rate of 1.0×10^{-3} mm³/N·m. The addition of Mo resulted in a gradual decrease in the specific wear rate of the deposits, and the wear rate was down by 17.4%, 80.6%, and 94.9% for the Mo_{0.2}, Mo_{0.5}, and Mo_{1.0} deposits. Table 3 summarizes the specific wear rate of CoCrFeNiMo_x HEAs fabricated by different manufacturing methods. It can be found that the specific wear rate exhibits a downward trend with the increase in the ratio of the Mo element. In addition, the wear resistance of the cold-sprayed CoCrFeNiMo_x HEA deposits is comparable or even superior to their counterparts. The significantly improved wear resistance can be attributed to the enhanced hardness induced by solid solution strengthening and the precipitation of hard phases [37].

3.4. Worn surface morphology and wear mechanism

To unveil the wear mechanisms of the cold-sprayed CoCrFeNiMo_x HEA deposits, the morphology and chemical composition of the worn surface were examined by using SEM and EDS. Fig. 10 shows the

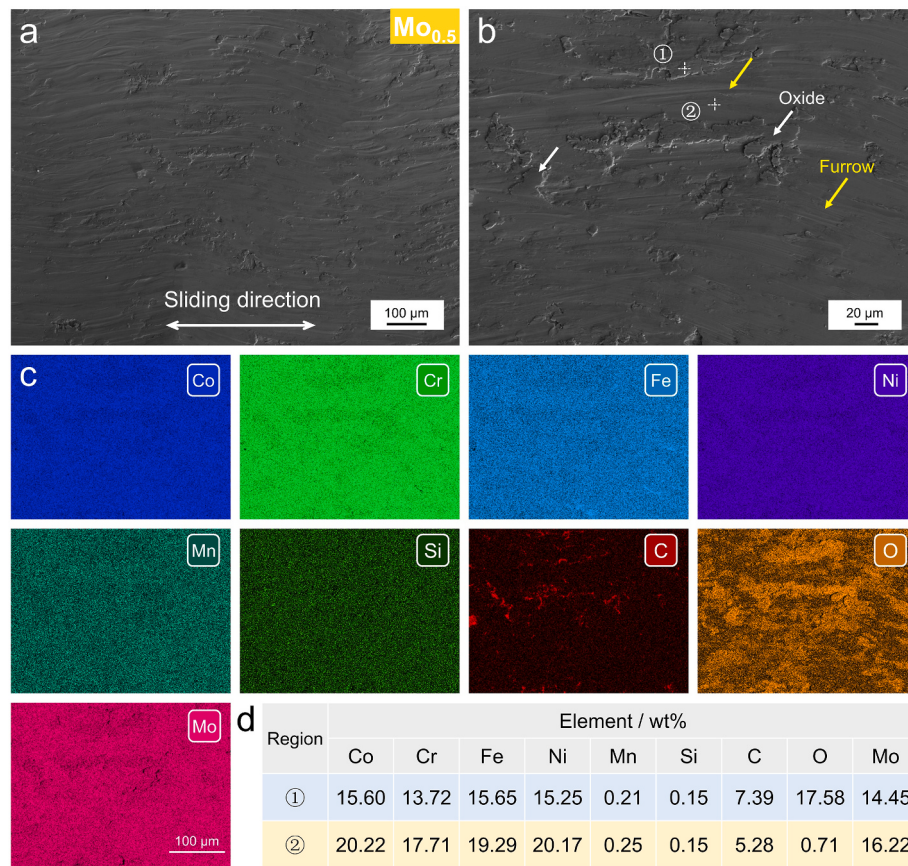


Fig. 12. Representative worn surface morphology and EDS results of the cold-sprayed CoCrFeNiMo_{0.5} HEA deposit. (a) and (b) SEM images, (c) and (d) EDS mapping and points analysis.

representative worn surface morphology of the Mo₀ HEA deposit. The worn surface exhibited scratches and furrows (see Fig. 10a and b) along the sliding direction, which were the typical features of abrasive wear. In addition, some dark-layered structures attached to the worn surface can be observed, as indicated by the white arrows in Fig. 10b. The EDS mapping (see Fig. 10c) shows that such a layered structure was oxygen-rich, suggesting that the layered structure was composed of oxides. Quantitatively, a high oxygen element content (17.49 wt%) was detected at position 1 on the oxidation layer, while the oxygen element content was only 1.28 wt% on the worn surface (see position 2). The formation of the oxidation layer on the worn surface can be attributed to the accumulation of heat generated by frictional interaction between the deposit surface and grinding ball and plastic deformation during the wear process [44]. The dark oxide layer was full of micro-cracks and nonuniformly distributed on the worn surface, which resulted in poor wear resistance [45]. Furthermore, the detection of Mn, Si, and C elements on the worn surface indicated that the material from the GCr15 ball transferred to the worn surface of the Mo₀ deposit (see Fig. 10c and d), which exhibited adhesive wear characteristics.

Fig. 11 shows the representative worn surface morphology of the cold-sprayed Mo_{0.2} HEA deposit. Compared to the worn surface of the Mo₀ deposit, the furrows became narrowed and shallowed, implying improved wear resistance. Moreover, the shape of the oxide changed from large-sized lamellae to small fragments, and the number of oxides on the worn surface also dramatically decreased, as shown in Fig. 11a and b. The EDS results show that the oxygen element content at position 1 (oxide) and position 2 (worn surface) was 16.97 % and 4.25%, respectively. The elements of Mn, Si, and C can also be identified on the worn surface, which is the feature of adhesive wear. The wear mechanism of Mo_{0.2} is dominated by abrasive wear, adhesive wear, and oxidative wear. From the representative worn surface morphology of the

Mo_{0.5} HEA deposit (see Fig. 12), the worn surface became smooth, and the width and depth of the furrows were significantly reduced. This suggests the improvement of wear resistance of the Mo_{0.5} deposit, which can also be demonstrated by the dramatically decreased specific wear rate, as shown in Fig. 9b. Moreover, fewer oxides were visible although the oxygen element was widely distributed on the worn surface.

Fig. 13 exhibits the representative worn surface morphology of the cold-sprayed Mo_{1.0} HEA deposit. The furrows parallel to the sliding direction (as pointed by the yellow arrows in Fig. 13b), and the detection of elements from the GCr15 ball (see Fig. 13c) indicated the abrasive wear and adhesive wear characteristics. In addition, the particle-particle boundaries were clearly visible, which was dramatically different from the worn surfaces of the other deposits. It can be found that the majority of particles were near-spherical after deposition due to the high deformation resistance of the material. Moreover, some particles were completely peeled off from the deposit surface, as shown in Fig. 13b. The detection of Cu element in the EDS mapping indicated that localized base metal was exposed after the wear test despite the lowest specific wear rate of the deposit (see Fig. 9b). This can be attributed to the limited thickness of the Mo_{1.0} deposit (~0.1 mm). The increase in the Mo ratio in CoCrFeNiMo_x HEA powders can indeed enhance the wear resistance of the cold-sprayed deposits, but this also increases the difficulty of particle deposition at the same time due to the high deformation resistance and brittle characteristics.

Fig. 14 shows the cross-sectional morphology of the wear tracks of the cold-sprayed CoCrFeNiMo_x HEA deposits. A continuous oxide layer with a thickness of ~6.5 μm was formed on the worn surface of the Mo₀ deposit, as shown in Fig. 14a. The formation of oxide layers can be attributed to the increased temperature on the deposit surface over time. As the sliding friction proceeded, the oxide layers got worn due to fatigue on the surface, and the oxide layers were broken into small blocks

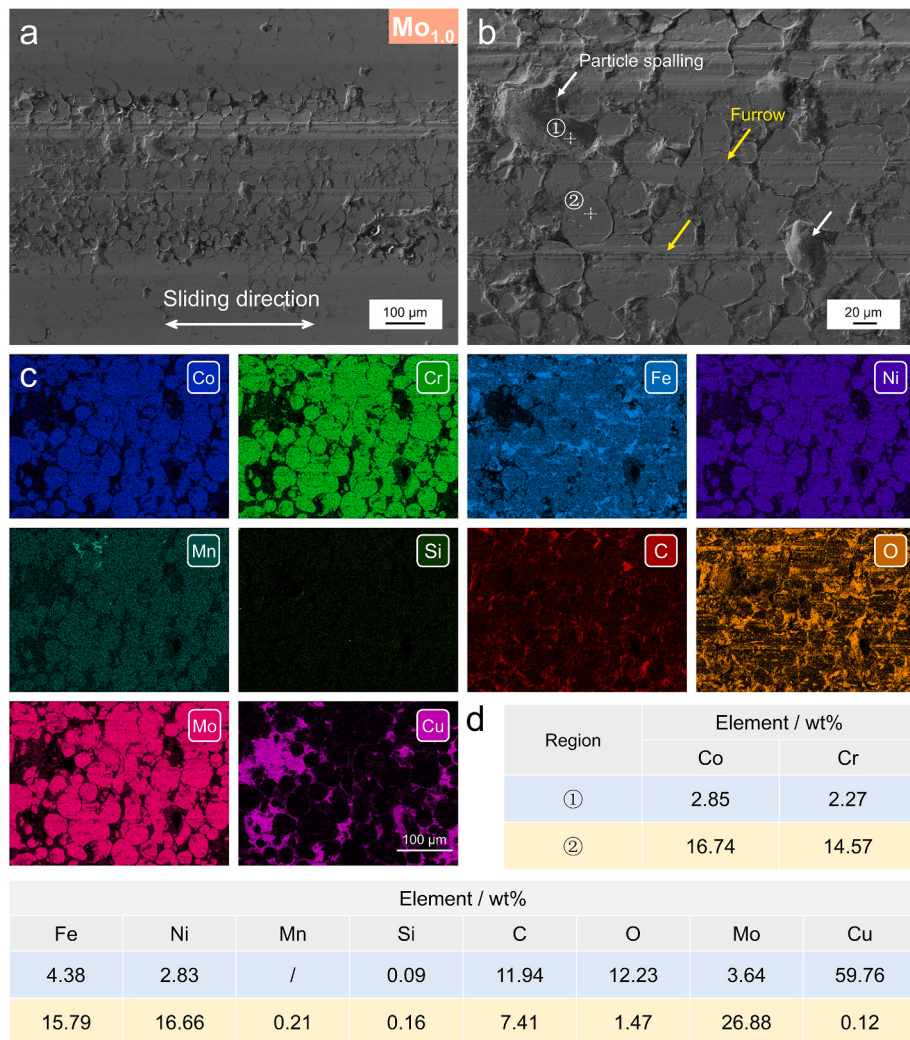


Fig. 13. Representative worn surface morphology and EDS results of the cold-sprayed CoCrFeNiMo_{1.0} HEA deposit. (a) and (b) SEM images, (c) and (d) EDS mapping and points analysis.

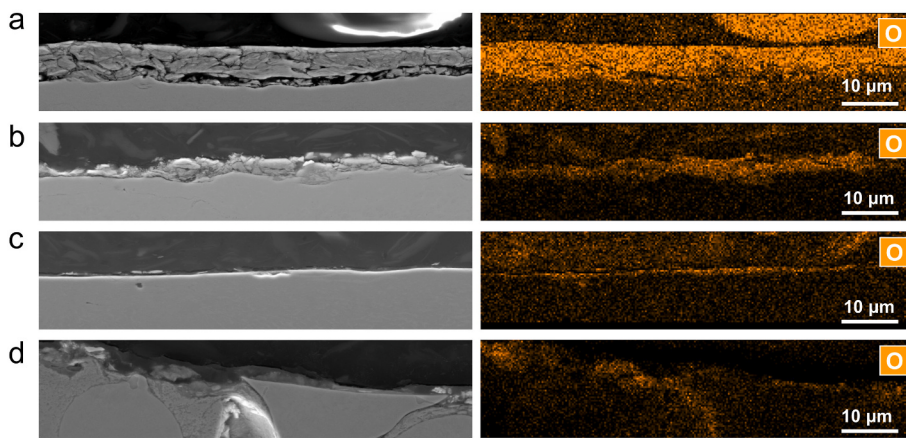


Fig. 14. Cross-sectional morphology of the wear tracks of the cold-sprayed CoCrFeNiMo_x HEA deposits. (a) Mo₀, (b) Mo_{0.2}, (c) Mo_{0.5}, (d) Mo_{1.0}.

with visible micro-cracks. The Mo_{0.2} deposit also shows the formed oxide layer, which was discontinuous and thinner compared to that of the Mo₀ deposit (see Fig. 14b). This can be attributed to the oxidation resistance feature of the molybdenum element [46]. For the Mo_{0.5} deposit, the oxide layer became indistinguishable from the SEM image, and

only a thin oxide layer (~1 μm) was formed at the top of the deposit according to the EDS mapping (see Fig. 14c). With regard to the Mo_{1.0} deposit, no oxide layer was formed on the top layer of the deposit, as shown in Fig. 14d. Therefore, the wear mechanisms of the cold-sprayed CoCrFeNiMo_x HEA deposits are abrasive wear, adhesive wear, and

oxidative wear when the Mo ratio is relatively low (e.g., Mo₀ and Mo_{0.2}) and dominated by the abrasive wear and adhesive wear with the further increase in Mo ratio (e.g., Mo_{0.5} and Mo_{1.0}).

4. Conclusion

In this work, Mo-doped CoCrFeNi high-entropy alloys (HEAs) were manufactured by solid-state cold spray deposition process to intentionally improve the wear resistance of CoCrFeNi HEAs. The microstructural evolution, phase structure, nanomechanical property, and wear resistance properties of the cold-sprayed CoCrFeNiMo_x HEA deposits were systematically investigated. The cold-sprayed CoCrFeNiMo_x HEA deposits presented microscale heterogeneity due to the unavoidable defects and heterostructure. The Mo_{0.2} and Mo_{0.5} deposits were identified as single FCC solid solution structures as the Mo₀ deposit, while the sigma (σ) phase and mu (μ) phase were precipitated in the FCC matrix for the Mo_{1.0} deposit. The doping of Mo element into cold-sprayed CoCrFeNiMo_x HEAs significantly increased the global nanohardness from 5.01 GPa (Mo₀ deposit) to 10.02 GPa (Mo_{1.0} deposit) due to the synergistic effects of solid solution strengthening and precipitation strengthening. This makes the Mo_{1.0} deposit exhibit the lowest specific wear rate of 5.1×10^{-5} mm³/N·m, which decreased by 94.90% compared with that of the Mo₀ deposit. The wear mechanisms of Mo₀ and Mo_{0.2} deposits were dominated by abrasive wear, adhesive wear, and oxidative wear, while for the Mo_{0.5} and Mo_{1.0} deposits, the wear mechanisms were mainly abrasive wear and adhesive wear. However, the increased Mo ratio in CoCrFeNiMo_x HEA powders significantly made it difficult to deposit due to the increased deformation resistance and brittle characteristics, particularly for Mo_{1.0} powder. This was reflected in the extremely limited deposit thickness (~ 0.1 mm) even though high processing parameters were applied. This could lead to premature failure of the wear-resistance deposit under extreme working conditions. The current study has shown that the doping of Mo element into CoCrFeNi HEA can significantly enhance the wear resistance properties with the increase in Mo ratio. However, the trade-off between the Mo content and the depositability of material should be taken into consideration.

Declaration of competing interest

The authors declare that they have no known competing financial interests or personal relationships that could have appeared to influence the work reported in this paper.

Acknowledgements

Mr. Ningsong Fan would like to acknowledge the financial support from the China Scholarship Council (CSC) – Trinity College Dublin Joint Scholarship Programme (No. 201906460020). Dr. Shuo Yin acknowledges the fund from the State Key Laboratory of Solidification Processing, NPU, China) (SKLSP202011, 2022-TZ-01). Dr. Yingchun Xie acknowledges the financial support from the National Key R&D Program (2023YFE0108000) and GDAS' project of Science and Technology Development (2022GDASZH-2022010203-003). The authors also would like to thank the Advanced Microscopy Laboratory (AML) of Trinity College Dublin for the support in data analysis.

References

- [1] Ye YF, Wang Q, Lu J, Liu CT, Yang Y. High-entropy alloy: challenges and prospects. *Mater Today* 2016;19:349–62. <https://doi.org/10.1016/j.mattod.2015.11.026>.
- [2] George EP, Curtin WA, Tasan CC. High entropy alloys: a focused review of mechanical properties and deformation mechanisms. *Acta Mater* 2020;188: 435–74. <https://doi.org/10.1016/j.actamat.2019.12.015>.
- [3] Gao MC, Yeh J-W, Liaw PK, Zhang Y. High-entropy alloys. first ed. Springer International Publishing; 2016. <https://doi.org/10.1007/978-3-319-27013-5>.
- [4] Ren H, Chen RR, Gao XF, Liu T, Qin G, Wu SP, et al. High-performance AlCoCrFeNi high entropy alloy with marine application perspective. *J Mater Res Technol* 2023; 25:6751–63. <https://doi.org/10.1016/j.jmrt.2023.07.135>.
- [5] Ren H, Chen RR, Liu T, Gao XF, Qin G, Wu SP, et al. Unraveling the oxidation mechanism of Y-doped AlCoCrFeNi high-entropy alloy at 1100 °C. *Appl Surf Sci* 2024;652. <https://doi.org/10.1016/j.apsusc.2024.159316>.
- [6] Jin B, Zhang N, Yin S. Strengthening behavior of AlCoCrFeNi(TiN)x high-entropy alloy coatings fabricated by plasma spraying and laser remelting. *J Mater Sci Technol* 2022;121:163–73. <https://doi.org/10.1016/j.jmst.2021.12.055>.
- [7] Arif ZU, Khalid MY, ur Rehman E, Ullah S, Atif M, Tariq A. A review on laser cladding of high-entropy alloys, their recent trends and potential applications. *J Manuf Process* 2021;68:225–73. <https://doi.org/10.1016/j.jmapro.2021.06.041>.
- [8] Pogrebnyak AD, Bagdasaryan AA, Yakushchenko IV, Beresnev VM. The structure and properties of high-entropy alloys and nitride coatings based on them. *Russ Chem Rev* 2014;83:1027–61. <https://doi.org/10.1070/rctr4407>.
- [9] Padamata SK, Yasinskiy A, Yanov V, Saevardsdottir G. Magnetron sputtering high-entropy alloy coatings: a mini-review. *Metals* 2022;12:319. <https://doi.org/10.3390/met12020319>.
- [10] Kuptsov KA, Antonyuk MN, Shevchenko AN, Bondarev AV, Ignatov SG, Slukin PV, et al. High-entropy Fe-Cr-Ni-Co-(Cu) coatings produced by vacuum electro-spark deposition for marine and coastal applications. *Surf Coating Technol* 2023;453: 129136. <https://doi.org/10.1016/j.surfcoat.2022.129136>.
- [11] Meghwal A, Anupam A, Murty BS, Berndt CC, Kottada RS, Ang ASM. Thermal spray high-entropy alloy coatings: a review. *J Therm Spray Technol* 2020;29:857–93. <https://doi.org/10.1007/s11666-020-01047-0>.
- [12] Pogrebnyak AD, Tyurin YN. Modification of material properties and coating deposition using plasma jets. *Phys Usp* 2005;48:487–514. <https://doi.org/10.1070/pu2005v04n05abeh002055>.
- [13] Supekar R, Nair RB, McDonald A, Stoyanov P. Sliding wear behavior of high entropy alloy coatings deposited through cold spraying and flame spraying: a comparative assessment. *Wear* 2023;516–517:204596. <https://doi.org/10.1016/j.wear.2022.204596>.
- [14] Zhu J, Cheng X, Zhang L, Hui X, Wu Y, Zheng H, et al. Microstructures, wear resistance and corrosion resistance of CoCrFeNi high entropy alloys coating on AZ91 Mg alloy prepared by cold spray. *J Alloys Compd* 2022;925:166698. <https://doi.org/10.1016/j.jallcom.2022.166698>.
- [15] Silvello A, Cavaliere P, Yin S, Lupoi R, Garcia Cano I, Dosta S. Microstructural, mechanical and wear behavior of HVOF and cold-sprayed high-entropy alloys (HEAs) coatings. *J Therm Spray Technol* 2022. <https://doi.org/10.1007/s11666-021-01293-w>.
- [16] Yin S, Fan N, Huang C, Xie Y, Zhang C, Lupoi R, et al. Towards high-strength cold spray additive manufactured metals: methods, mechanisms, and properties. *J Mater Sci Technol* 2024;170:47–64. <https://doi.org/10.1016/j.jmst.2023.05.047>.
- [17] Poza P, Angel M. Cold-sprayed coatings: microstructure, mechanical properties, and wear behaviour. *Prog Mater Sci* 2022;123:100839. <https://doi.org/10.1016/j.pmatsci.2021.100839>.
- [18] Lehtonen J, Koivuluoto H, Ge Y, Juselius A, Hannula S-P. Cold gas spraying of a high-entropy CrFeNiMn equiatomic alloy. *Coatings* 2020;10:53. <https://doi.org/10.3390/coatings10010053>.
- [19] Lin D, Xu L, Jing H, Han Y, Zhao L, Minami F. Effects of annealing on the structure and mechanical properties of FeCoCrNi high-entropy alloy fabricated via selective laser melting. *Addit Manuf* 2020;32:101058. <https://doi.org/10.1016/j.addma.2020.101058>.
- [20] Zhao W, Han J-K, Kuzminova YO, Evlashin SA, Zhilyaev AP, Pesin AM, et al. Significance of grain refinement on micro-mechanical properties and structures of additively-manufactured CoCrFeNi high-entropy alloy. *Mater Sci Eng, A* 2021;807: 140898. <https://doi.org/10.1016/j.msea.2021.140898>.
- [21] Fan N, Rafferty A, Lupoi R, Li W, Xie Y, Yin S. Microstructure evolution and mechanical behavior of additively manufactured CoCrFeNi high-entropy alloy fabricated via cold spraying and post-annealing. *Mater Sci Eng, A* 2023;873: 144748. <https://doi.org/10.1016/j.msea.2023.144748>.
- [22] Chen X-R, Zhai Q-J, Dong H, Dai B-H, Mohrbacher H. Molybdenum alloying in cast iron and steel. *Adv Manuf* 2020;8:3–14. <https://doi.org/10.1007/s40436-019-00282-1>.
- [23] Qin G, Chen R, Zheng H, Fang H, Wang L, Su Y, et al. Strengthening FCC-CoCrFeMnNi high entropy alloys by Mo addition. *J Mater Sci Technol* 2019;35: 578–83. <https://doi.org/10.1016/j.jmst.2018.10.009>.
- [24] Liu WH, Lu ZP, He JY, Luan JH, Wang ZJ, Liu B, et al. Ductile CoCrFeNiMox high entropy alloys strengthened by hard intermetallic phases. *Acta Mater* 2016;116: 332–42. <https://doi.org/10.1016/j.actamat.2016.06.063>.
- [25] Liu Y, Xie Y, Cui S, Yi Y, Xing X, Wang X, et al. Effect of mo element on the mechanical properties and tribological responses of cocrnenimox high-entropy alloys. *Metals* 2021;11:1–18. <https://doi.org/10.3390/met11030486>.
- [26] Oliver WC, Pharr GM. An improved technique for determining hardness and elastic modulus using load and displacement sensing indentation experiments. *J Mater Res* 1992;7:1564–83. <https://doi.org/10.1557/JMR.1992.1564>.
- [27] Archard JF. Contact and rubbing of flat surfaces. *J Appl Phys* 1953;24:981–8. <https://doi.org/10.1063/1.1721448>.
- [28] Ungár T. Microstructural parameters from X-ray diffraction peak broadening. *Scripta Mater* 2004;51:777–81. <https://doi.org/10.1016/j.scriptamat.2004.05.007>.
- [29] Deng G, Tieu AK, Su L, Wang P, Wang L, Lan X, et al. Investigation into reciprocating dry sliding friction and wear properties of bulk CoCrFeNiMo high entropy alloys fabricated by spark plasma sintering and subsequent cold rolling

- processes: role of Mo element concentration. *Wear* 2020;460–1. <https://doi.org/10.1016/j.wear.2020.203440>.
- [30] Shun T-T, Chang L-Y, Shiu M-H. Microstructure and mechanical properties of multiprincipal component CoCrFeNiMox alloys. *Mater Char* 2012;70:63–7. <https://doi.org/10.1016/j.matchar.2012.05.005>.
- [31] Mukarram M, Munir MA, Mujahid M, Yaqoob K. Systematic development of eutectic high entropy alloys by thermodynamic modeling and experimentation: an example of the cocrfeni-mo system. *Metals* 2021;11. <https://doi.org/10.3390/met11091484>.
- [32] Guo S, Ng C, Lu J, Liu CT. Effect of valence electron concentration on stability of fcc or bcc phase in high entropy alloys. *J Appl Phys* 2011;109:103505. <https://doi.org/10.1063/1.3587228>.
- [33] Guo S, Liu CT. Phase stability in high entropy alloys: formation of solid-solution phase or amorphous phase. *Prog Nat Sci Mater Int* 2011;21:433–46. [https://doi.org/10.1016/S1002-0071\(12\)60080-X](https://doi.org/10.1016/S1002-0071(12)60080-X).
- [34] Tsai M-H, Tsai K-Y, Tsai C-W, Lee C, Juan C-C, Yeh J-W. Criterion for sigma phase formation in Cr- and V-containing high-entropy alloys. *Mater Res Lett* 2013;1:207–12. <https://doi.org/10.1080/21663831.2013.831382>.
- [35] Leyland A, Matthews A. On the significance of the H/E ratio in wear control: a nanocomposite coating approach to optimised tribological behaviour. *Wear* 2000;246:1–11. [https://doi.org/10.1016/S0043-1648\(00\)00488-9](https://doi.org/10.1016/S0043-1648(00)00488-9).
- [36] Zambrano OA, Muñoz EC, Rodríguez SA, Coronado JJ. Running-in period for the abrasive wear of austenitic steels. *Wear* 2020;452–453:203298. <https://doi.org/10.1016/j.wear.2020.203298>.
- [37] Zhou C, Wang S, Wang G, Zhang J, Liu W. Investigation on the microstructure, wear and corrosion resistance of FeCoNiCrMox high-entropy alloy coatings deposited on 40Cr by laser cladding. *J Mater Sci* 2022;57:18615–39. <https://doi.org/10.1007/s10853-022-07684-w>.
- [38] Wu H, Zhang S, Wang ZY, Zhang CH, Chen HT, Chen J. New studies on wear and corrosion behavior of laser cladding FeNiCoCrMox high entropy alloy coating: the role of Mo. *Int J Refract Met Hard Mater* 2022;102:105721. <https://doi.org/10.1016/j.ijrmhm.2021.105721>.
- [39] Li K, Liang J, Zhou J. Microstructure and elevated temperature tribological performance of the CoCrFeNiMo high entropy alloy coatings. *Surf Coating Technol* 2022;449:128978. <https://doi.org/10.1016/j.surfcoat.2022.128978>.
- [40] Sha M, Wang S, Li S, Jia C, Huang T, Zhu X, et al. Effect of Mo on microstructure and properties of AlCoCrFeNiMox high entropy alloy coatings prepared by laser cladding. *Mater Res Express* 2023;10:126514. <https://doi.org/10.1088/2053-1591/ad1544>.
- [41] Lyu P, Peng T, Miao Y, Liu Z, Gao Q, Zhang C, et al. Microstructure and properties of CoCrFeNiMo0.2 high-entropy alloy enhanced by high-current pulsed electron beam. *Surf Coating Technol* 2021;410:126911. <https://doi.org/10.1016/j.surfcoat.2021.126911>.
- [42] Xiao JK, Li TT, Wu YQ, Chen J, Zhang C. Microstructure and tribological properties of plasma-sprayed CoCrFeNi-based high-entropy alloy coatings under dry and oil-lubricated sliding conditions. *J Therm Spray Technol* 2021;30:926–36. <https://doi.org/10.1007/s11666-021-01175-1>.
- [43] Deng C, Wang C, Chai L, Wang T, Luo J. Mechanical and chemical properties of CoCrFeNiMo0.2 high entropy alloy coating fabricated on Ti6Al4V by laser cladding. *Intermetallics* 2022;144:107504. <https://doi.org/10.1016/j.intermet.2022.107504>.
- [44] Sutter G, Ranc N. Flash temperature measurement during dry friction process at high sliding speed. *Wear* 2010;268:1237–42. <https://doi.org/10.1016/j.wear.2010.01.019>.
- [45] Li H, Li X, Jin C, Li Q, Ma Q, Hua K, et al. Mechanical and tribological performance of AlCr0.5NbTa_{1-x} (x = 0, 0.5, 1) refractory high-entropy alloys. *J Mater Sci Technol* 2023;156:241–53. <https://doi.org/10.1016/j.jmst.2023.02.016>.
- [46] Yun DW, Seo HS, Jun JH, Lee JM, Kim KY. Molybdenum effect on oxidation resistance and electric conduction of ferritic stainless steel for SOFC interconnect. *Int J Hydrogen Energy* 2012;37:10328–36. <https://doi.org/10.1016/j.ijhydene.2012.04.013>.